

Unilateral Silver-Loaded Silk Fibroin Difunctional Membranes as Antibacterial Wound Dressings

Jinlong Shao,[§] Yating Cui,[§] Ye Liang, Hong Liu, Baojin Ma,^{*} and Shaohua Ge^{*}Cite This: *ACS Omega* 2021, 6, 17555–17565

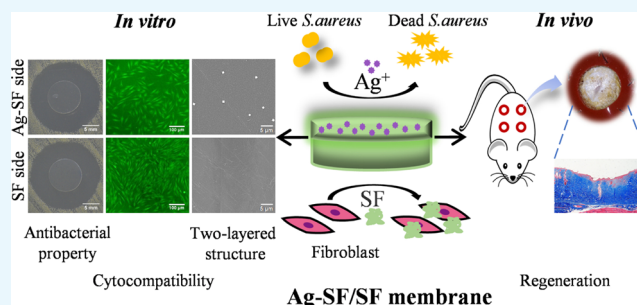
Read Online

ACCESS |

Metrics & More

Article Recommendations

ABSTRACT: Silk fibroin (SF) has been widely used as wound dressings due to its good biocompatibility. To enhance the antibacterial properties of the dressings, silver (Ag) is often added. However, an overdose of Ag may cause cytotoxicity and inhibit wound healing. Therefore, this study aimed to develop a two-layered membrane to reduce cytotoxicity while maintaining the antibacterial properties of Ag through a simplified layer-by-layer technique. The membranes comprised an Ag-rich SF layer (Ag-SF) and a pure SF layer. The unilateral Ag-loaded membranes showed efficient antibacterial properties at doses above 0.06 mg/mL Ag, and the antibacterial properties were comparable on both sides. In contrast, the SF sides of the membranes showed lower cytotoxicity than the Ag-SF sides of the membranes. Further studies on the thickness ratio of Ag-SF/SF layers revealed that Ag0.12-SF/SF membranes with a ratio of 1:3 had high cytocompatibility on the SF sides while holding a strong antibacterial property. Besides, the SF sides of the Ag0.12-SF/SF1:3 membranes promoted the expression levels of collagen I and transforming growth factor- β mRNA in human foreskin fibroblasts. The SF sides of the Ag0.12-SF/SF1:3 membranes significantly promoted the healing of infected wounds *in vivo*. Therefore, unilateral loading with the simplified layer-by-layer preparation technique provided an effective method to balance the cytotoxicity and the antibacterial property of Ag-loaded materials and thus form a broader therapeutic window for Ag applications. The unilateral Ag-loaded silk fibroin difunctional membranes have the potential to be further preclinically explored as wound dressings.



1. INTRODUCTION

Silk fibroin (SF) is a natural protein extracted from silk.¹ Due to the abilities to promote cell migration, proliferation, angiogenesis, and re-epithelialization, and other significant biological advantages, SF, with a similar structure to extracellular matrix (ECM), has been widely explored as wound dressings.^{2–5} Besides, these dressings are able to promote wound healing.³ Since most wounds are exposed to the environments directly, they are extremely susceptible to bacterial invasion. Therefore, preventing infection is another important issue for wound healing. However, SF *per se* does not have antibacterial effects.

Various methods have been proposed to endow SF with antibacterial properties. Chitosan,⁶ antibacterial peptides,⁷ silver (Ag) nanoparticles,⁸ zinc oxide,⁹ etc. are commonly added to SF to exert antibacterial effects. Among them, Ag has been widely explored in wound dressings, since it has broad-spectrum antibacterial properties and does not show widespread drug resistance like antibiotics.¹⁰ Studies have found that eukaryotic cells are more tolerant of Ag than prokaryotic cells.^{11,12} In prokaryotes, important biochemical pathways such as the respiratory chain or DNA replication are located at the cytoplasmic membrane, while the mitochondria and nucleus of eukaryotic cells are protected in cellular organelles.¹³ There-

fore, the difference between the cytotoxic and the antibacterial concentrations of Ag can be used as a therapeutic window for antibacterial applications.¹⁴

Nevertheless, the applications of Ag are controversial.¹⁵ Some researchers found that Ag-containing dressings delayed wound healing^{16,17} while others confirmed that Ag-containing dressings promoted wound healing.^{18,19} The pieces of literature have no consistent conclusions on the effect of Ag-containing dressings on wound healing. The possible reason is that Ag is a double-edged sword, which has antibacterial properties and is also toxic to cells.¹⁵ Therefore, how to reduce the side effect of Ag on cell viability while maintaining its high antibacterial capability is an urgent issue that needs to be addressed.

The current methods to reduce Ag cytotoxicity include green biosynthesis using plant extracts, fungi, etc.,²⁰ combina-

Received: April 16, 2021

Accepted: June 21, 2021

Published: June 30, 2021



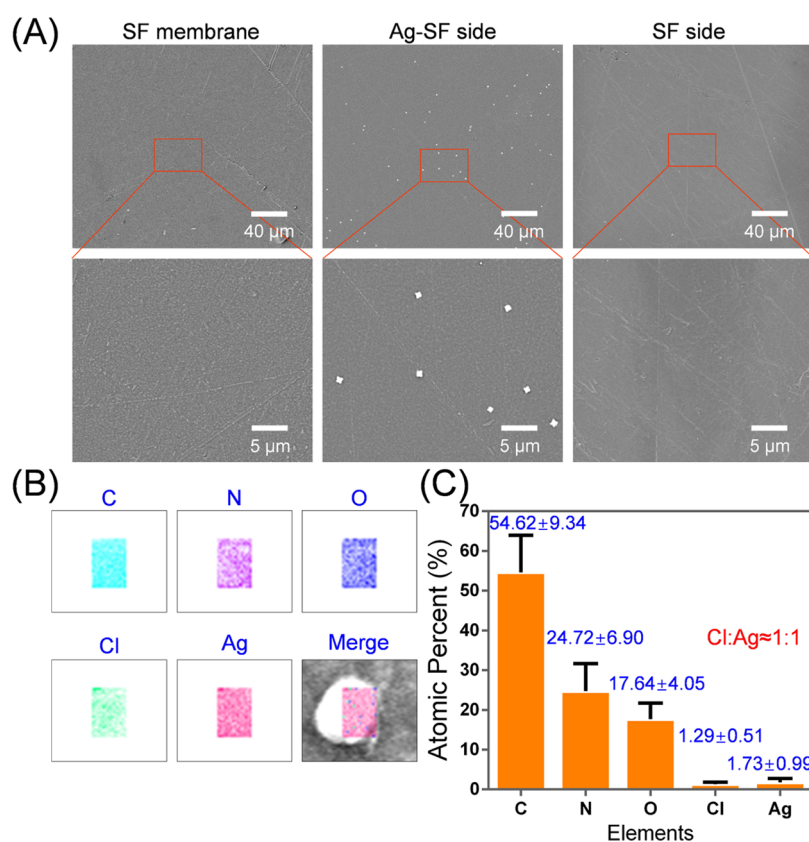


Figure 1. Morphological characterization and elemental analysis of SF and Ag-SF/SF membranes. (A) SEM images of the SF membrane and the Ag-SF side and SF side of Ag-SF/SF membrane with different magnifications. (B) Elements mapping and (C) atomic ratio of particles.

tion with antioxidants to reduce the level of reactive oxygen species (ROS) in cells,²¹ and preventing the release of Ag⁺ from the cathodic Ag by sacrificial anodic Fe.²² The layer-by-layer technique is a method for depositing thin films to generate functional materials with controlled structures, performances, and functions for various applications.^{23,24} Inspired by this, we proposed a simplified layer-by-layer technique that composited an SF layer on the Ag-loaded SF membrane. The prepared two-layer structure was further explored whether it could reduce the cytotoxicity of Ag while keeping its antibacterial effect.

To this end, a two-layered membrane with both a Ag-rich SF (Ag-SF) layer and a pure SF layer was designed and fabricated. The morphologies, physicochemical properties, and Ag⁺ release profiles of the membranes were characterized. The antimicrobial activity of Ag-SF/SF membranes with different Ag contents was evaluated by antibacterial experiments. Human foreskin fibroblasts (HFFs) were inoculated onto Ag-SF/SF membranes to explore the cytocompatibility of the Ag-SF and SF sides. The influence of different thickness ratios of the Ag-SF layer to the SF layer on cell viability was explored to elucidate the effect of the double-layer structure on the reduction of Ag cytotoxicity. Besides, collagen (Col) I and transforming growth factor (TGF)- β mRNA expression levels of HFFs on the SF sides were measured by a quantitative real-time polymerase chain reaction (qRT-PCR). Finally, Ag-SF/SF membranes were implanted into the rat excisional wound splinting model challenged with *Staphylococcus aureus* to evaluate the effect on wound healing.

2. RESULTS AND DISCUSSION

2.1. Morphology Characterization and Elemental Analysis of SF and Ag-SF/SF Membranes. The morphology of SF and Ag-SF/SF membranes was characterized by scanning electron microscopy (SEM)–energy-dispersive X-ray (EDX) spectroscopy. SF and Ag-SF/SF membranes both showed a smooth surface (Figure 1A). Many particles appeared on the Ag-SF side but not on the SF side. The EDX results confirmed that the particles were rich in C, N, O, Cl, and Ag (Figure 1B), and the atomic ratio of Ag to Cl was close to 1:1 (Figure 1C), which indicates the formation of AgCl due to the reaction between AgNO₃ and CaCl₂. Elements C, N, and O were derived from SF, and elements Ag and Cl were derived from AgCl.²⁵ Therefore, membranes with a two-layered structure were successfully fabricated by the simplified layer-by-layer technique, providing a basis for subsequent research.

2.2. Phase, Mechanical Properties, and Ag⁺ Release Profiles of Ag-SF/SF Membranes. X-ray diffraction (XRD) patterns were obtained to investigate the crystalline phase of SF and AgCl (Figure 2A). There was a typical diffraction peak presented in the XRD spectra of the SF membrane at $2\theta = \sim 21^\circ$. This characteristic diffraction peak was also observed on the Ag-SF side of the Ag-SF/SF membrane, which can be attributed to the crystalline diffraction of silk II with the β -sheet structure.^{26,27} Meanwhile, there were several typical peaks of AgCl that appeared at $2\theta = 27.8, 32.2,$ and 46.2° , which can be indexed to the (111), (200), and (220) planes, respectively (JCPDS no. 85-1355).²⁸ Consistent with the XRD pattern, the characteristic peaks of SF and Ag-SF/SF membranes at 1517 and 1623 cm⁻¹ (Figure 2B) in the Fourier

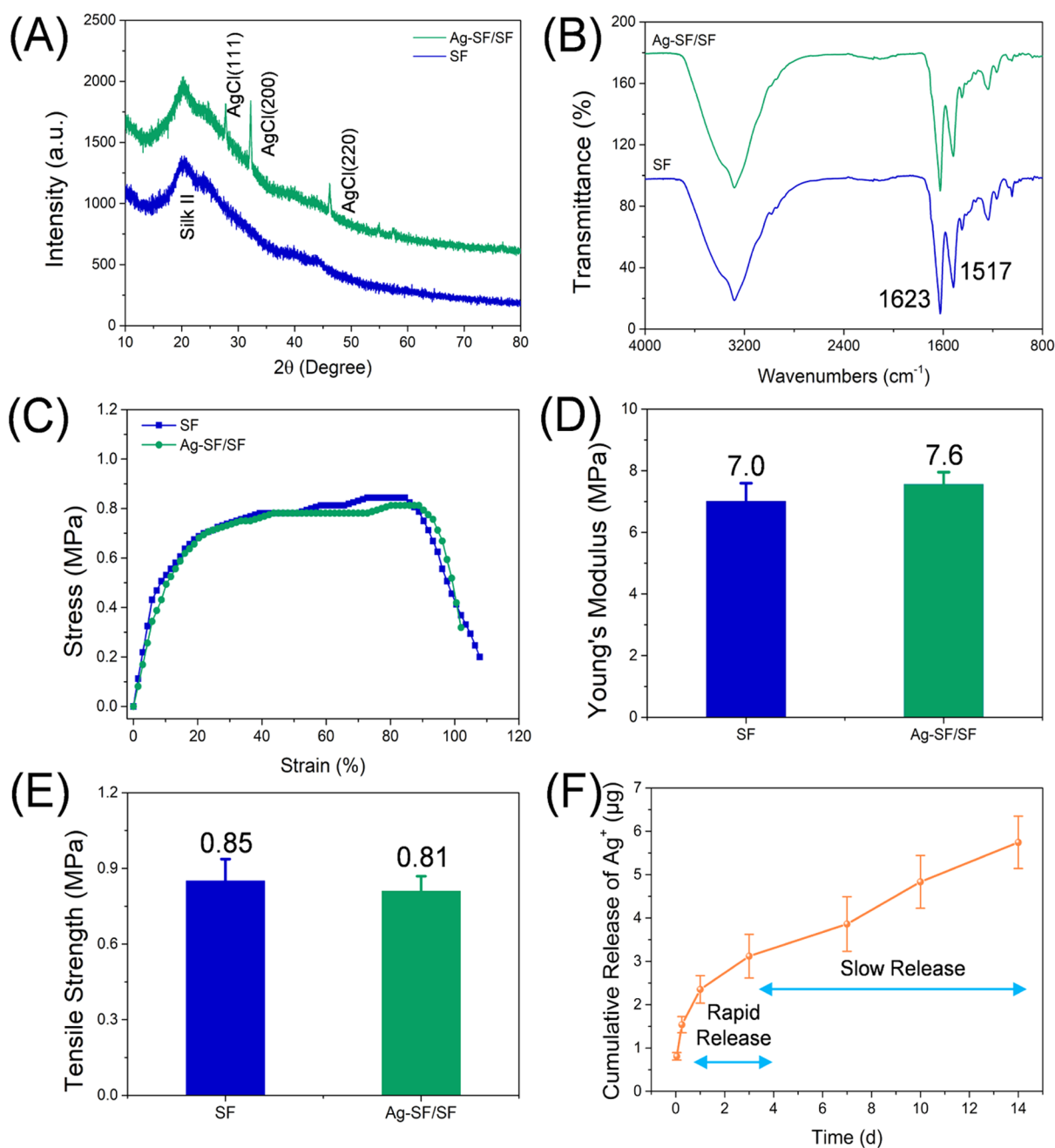


Figure 2. Phase and mechanical properties of SF and Ag-SF/SF membranes and Ag^+ release of Ag-SF/SF membranes. (A) XRD patterns and (B) FTIR spectra of SF and Ag-SF/SF membranes. (C–E) Mechanical properties of SF and Ag-SF/SF membranes. (F) Ag^+ release curve of Ag-SF/SF membranes.

transform infrared (FTIR) spectra belonged to the vibrations of amide II and I, respectively, which also confirmed the existence of the β -sheet structure in Ag-SF/SF membranes.²⁹ The addition of Ag did not change the structure of SF.

Since skin is elastic and has a certain range of motion, wound dressings should have a certain tensile strength.³⁰ As shown in Figure 2C–E, the Young moduli and tensile strengths of SF and Ag-SF/SF groups were similar. The prepared SF and Ag-SF/SF membranes both had high tensile modulus (~ 7.6 MPa), which was close to the 8 MPa in the previous study, indicating that the tensile strength of the Ag-SF/SF membrane was similar to that of the natural skin tissue,^{31,32} and the β -sheet structure formed by ethanol treatment enhanced mechanical properties.³³ Besides, the

addition of Ag endowed the membranes with antibacterial activity and AgCl particles apparently formed in situ. As shown in Figure 2F, in the early stage, Ag^+ exhibited a burst release, while the internal Ag^+ released relatively slowly in the later stage. Also, the cumulative release amount of 14 days accounted for about 25% of the total membrane. The release curve indicated that the release rate of Ag^+ slowed down gradually, which may provide a relatively long-term antibacterial property.

2.3. Antibacterial Property of Ag-SF/SF Membranes.

The antibacterial assessment of Ag-SF/SF was quantitatively evaluated by a zone of inhibition (ZOI) test. In the ZOI test of the samples against *S. aureus*, the Ag0.03-SF/SF membrane did not show a ZOI, but for Ag0.06-SF/SF, an obvious ZOI was

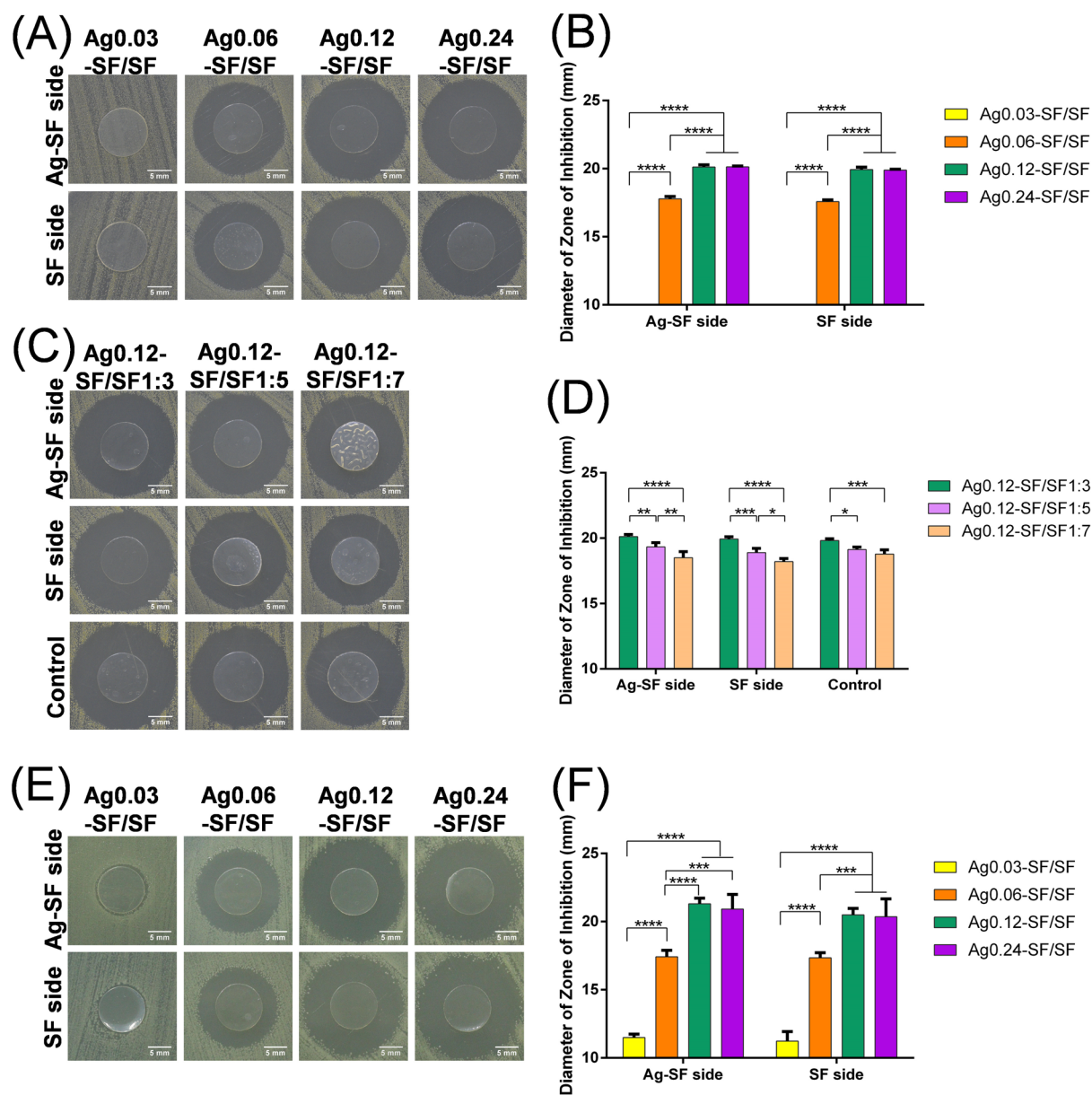


Figure 3. ZOI test of the samples against *S. aureus* (A–D) and *E. coli* (E, F). (A) Representative photos of the Ag-SF side and SF side of ZOI in Ag-SF/SF samples with different Ag concentrations. (B) Quantitative analysis of ZOI in Ag-SF/SF samples. (C) Representative photos of the Ag-SF side, SF side, and control of ZOI in Ag0.12-SF/SF samples with different thickness ratios. The single-layered membranes with Ag homogeneous distribution were set as the control. (D) Quantitative analysis of ZOI in Ag0.12-SF/SF samples with different thickness ratios. (E) Representative photos of the Ag-SF side and SF side of ZOI in Ag-SF/SF samples with different Ag concentrations. (F) Quantitative analysis of ZOI in Ag-SF/SF samples. The diameter of the samples was 10 mm. * $P < 0.05$, ** $P < 0.01$, *** $P < 0.001$, and **** $P < 0.0001$.

observed (Figure 3A), which indicated that the antibacterial properties of different membranes were dose-dependent, consistent with previous studies.^{15,34} The antibacterial efficacy gradually increased with an increased Ag amount, but the Ag0.12-SF/SF membrane showed a comparable antibacterial effect to the Ag0.24-SF/SF membrane (Figure 3B), which might be attributed to the fact that the released Ag^+ content reached saturation due to the precipitation–dissolution equilibrium of AgCl and Ag^+ -confined diffusion on the nutrient agar plate. To further elucidate the effect of layer thickness ratio on antibacterial efficacy, the membranes with different thickness ratios of the Ag-SF layer to the SF layer were tested and the single-layered membranes with Ag homogeneous distribution were set as the control. As shown

in Figure 3C, both the two-layered membranes and the single-layered membranes with Ag uniform distribution showed an obvious ZOI. Surprisingly, the SF sides and Ag-SF sides of the membranes showed similar antibacterial efficacy, regardless of the thickness ratio of Ag-SF/SF. It may be related to the diffusion of Ag^+ , which is accepted as the major antibacterial component of Ag-loaded materials.³⁵ Although the bacteria did not directly contact Ag on the SF sides, the moist environment could facilitate the release of Ag^+ to exert the antibacterial function. Besides, the antibacterial property of the membranes gradually decreased with an increase of SF layer thickness, but there was no significant difference among the control group and Ag-SF side and SF side of the membranes with the same thickness ratio (Figure 3D). This result may be explained that

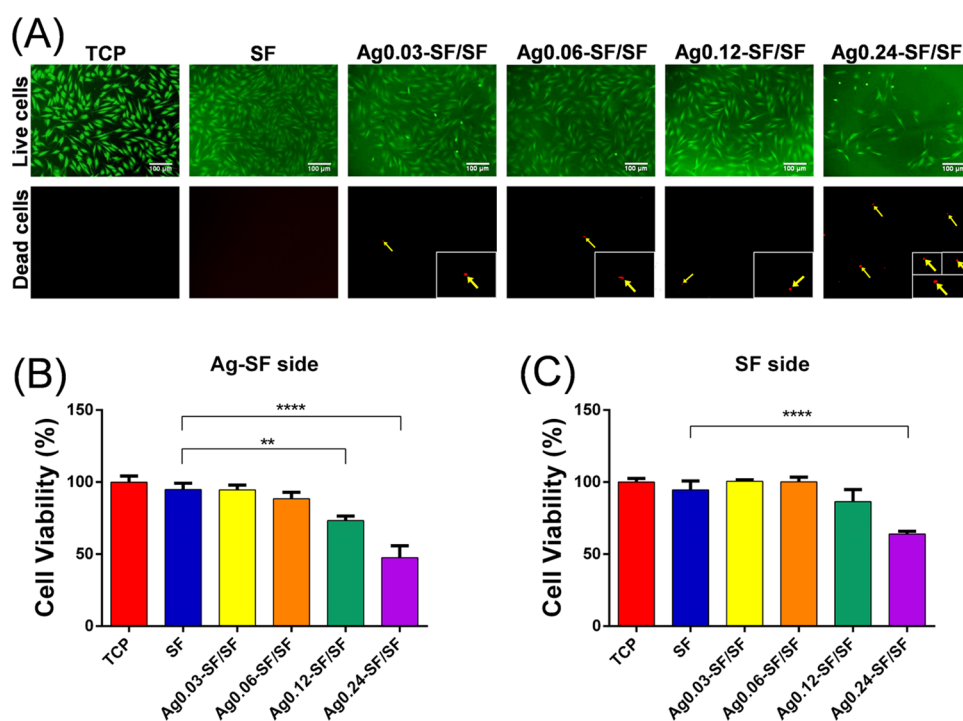


Figure 4. Cell viability detection. (A) Live/dead cell staining on SF membranes and Ag-SF side of Ag-SF/SF membranes after HFFs were seeded for 24 h. Yellow arrows indicated dead cells. (B, C) Effects of SF with Ag on the cell viability of HFFs for 24 h. (B) HFFs were seeded on the Ag-SF side. (C) HFFs were seeded on the SF side. ** $P < 0.01$ and **** $P < 0.0001$, compared with SF.

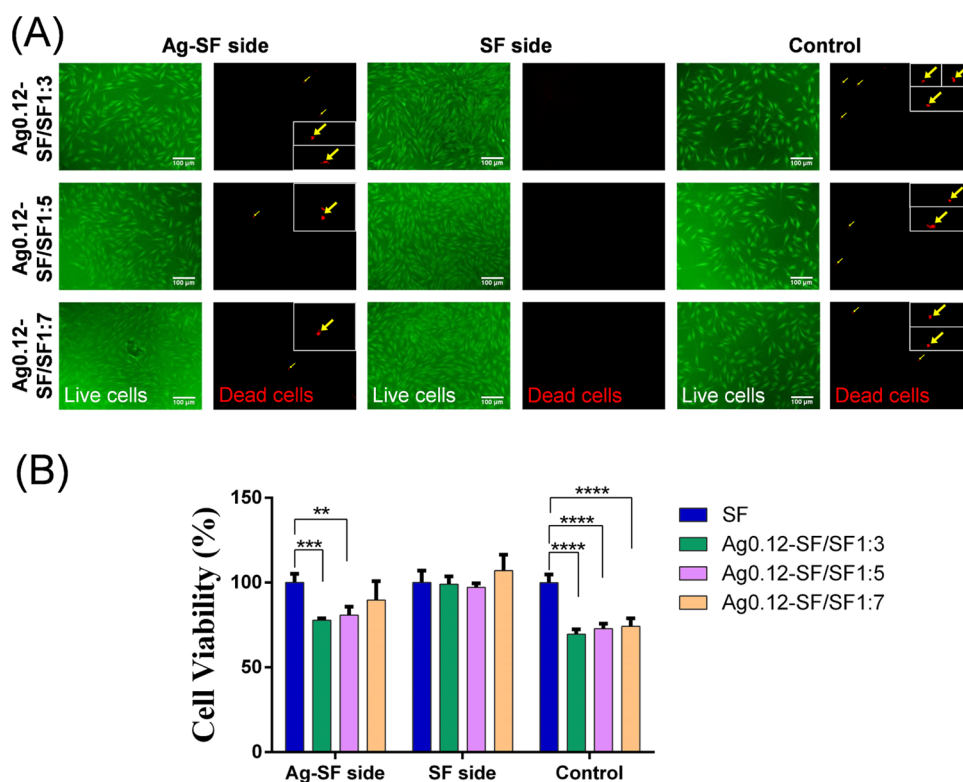


Figure 5. Cell viability detection on Ag0.12-SF/SF1:3, Ag0.12-SF/SF1:5, and Ag0.12-SF/SF1:7 membranes. (A) Live/dead cell staining on Ag0.12-SF/SF1:3, Ag0.12-SF/SF1:5, and Ag0.12-SF/SF1:7 membranes after HFFs were seeded for 24 h. Yellow arrows indicated dead cells. The single-layered membranes with Ag homogeneous distribution were set as the control. (B) Effects of different ratios of Ag-SF/SF on the cell viability of HFFs with different sides for 24 h. ** $P < 0.01$, *** $P < 0.001$, and **** $P < 0.0001$.

a thicker SF layer resulted in a lower Ag^+ concentration in the whole membranes and the antibacterial property of Ag was

dose-dependent. It may indicate that the dissolvable Ag^+ could diffuse freely in the SF layer, while the insoluble AgCl particles

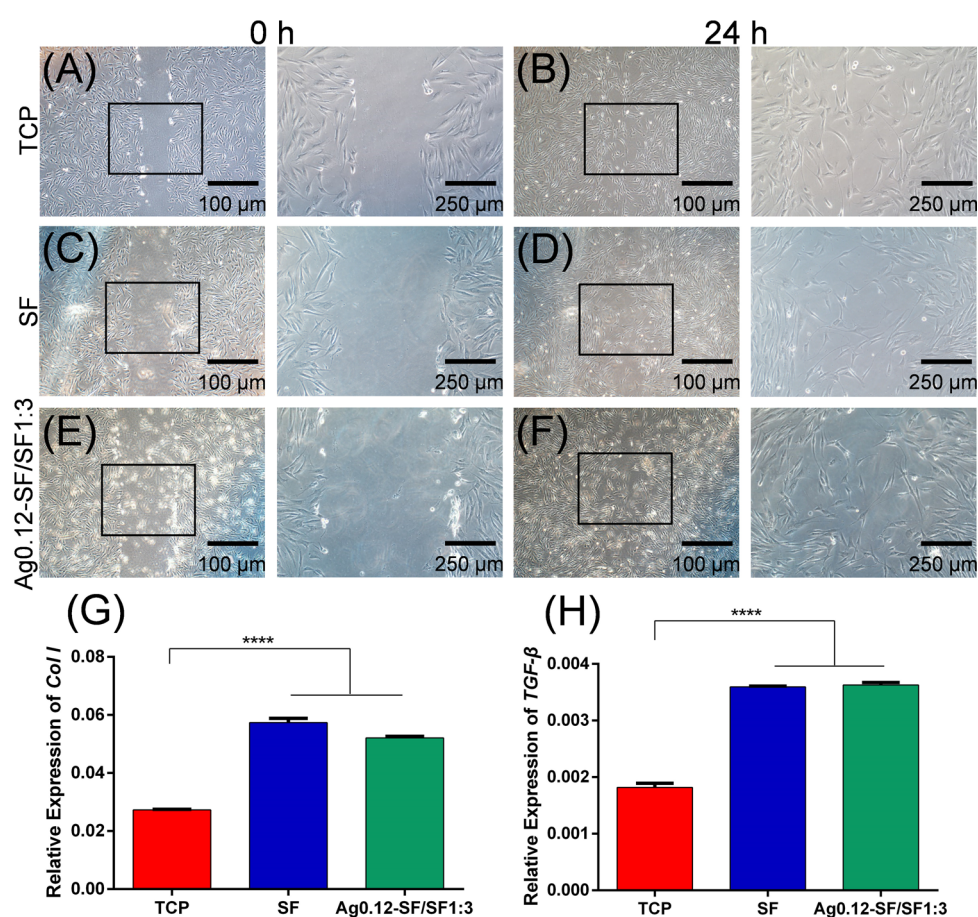


Figure 6. Scratch test and the gene expression result to evaluate *in vitro* wound healing. (A–F) Microscopic images of TCP, SF membrane, and the SF side of Ag0.12-SF/SF1:3 membrane groups at 0 and 24 h after an artificial injury with different magnifications. Relative expression levels of (G) Col I and (H) TGF-β at day 7. mRNA levels were evaluated by qRT-PCR and normalized to GAPDH mRNA expression. **** $P < 0.0001$, compared with TCP.

were relatively fixed in the Ag-SF layer. To prove the broad-spectrum antibacterial activity, we also tested the antibacterial effect of Ag-SF/SF1:3 membranes with different Ag concentrations against *Escherichia coli*. Similar to the results against *S. aureus*, both the Ag-SF side and SF side of Ag0.12-SF/SF1:3 membranes showed a good antibacterial effect on *E. coli* (Figure 3E,F). Therefore, Ag0.12-SF/SF1:3 membranes had high antibacterial efficacy on both Gram-positive and Gram-negative bacteria in skin wound infection.

2.4. Cell Viability on SF and Ag-SF/SF Membranes. To investigate the cytocompatibility of SF and Ag-SF/SF membranes, human foreskin fibroblasts (HFFs) seeded onto the membranes were observed by live/dead staining. As shown in Figure 4A, the live cells were dyed green, while dead cells were dyed red. The number of live cells decreased obviously and more dead cells appeared in the Ag0.24-SF/SF group compared to other groups. Moreover, cell viability on different sides of Ag-SF/SF membranes was further quantitatively assessed by the cell-counting kit-8 (CCK-8) kit. As shown in Figure 4B,C, the cytotoxicity of both sides of Ag-SF/SF membranes increased with an increase in Ag amount. Apparently, the viability of HFFs on the SF side was higher than that on the Ag-SF side, as evidenced by that the SF side of Ag0.12-SF/SF groups showed almost no cytotoxicity, while the Ag-SF side showed relatively significant cytotoxicity (Figure 4B,C). The results indicated that the two-layered structure could lower the cytotoxicity of Ag loaded within the

membranes. This decreased cytotoxicity of the two-layered membranes may be related to AgCl on different sides, as shown in SEM images. In addition, the cell viability test on the Ag-SF side showed that the cytotoxicity was dose-dependent, which agreed with a previous study.³⁶

2.5. Cell Viability on Membranes of Different Layer Thickness Ratios. Since the SF sides of the membranes showed better cytocompatibility than Ag-SF sides, we further explored the effects of different layer thickness ratios of Ag0.12-SF/SF, i.e., 1:3, 1:5, and 1:7. As shown in Figure 5A,B, compared with the membranes with a homogeneous distribution of Ag at equivalent content, the SF sides of Ag0.12-SF/SF membranes showed better cytocompatibility, while the Ag-SF sides showed comparable cytotoxicity. Therefore, our research revealed that even with a relatively thin layer of SF, the double-layer structure of unilateral Ag-loaded SF membranes could significantly improve the cytocompatibility of the SF side.

From the antibacterial test and cell viability evaluation, the SF sides of Ag0.12-SF/SF1:3 membranes showed the optimal effect among all tested settings with a relatively strong antibacterial efficacy and lower cytotoxicity. This could provide a therapeutic window. The concentration discrepancy between the antibacterial effect and cytotoxicity may be related to the fact that important biochemical pathways in eukaryotes are protected in cellular organelles, while prokaryotes do not have

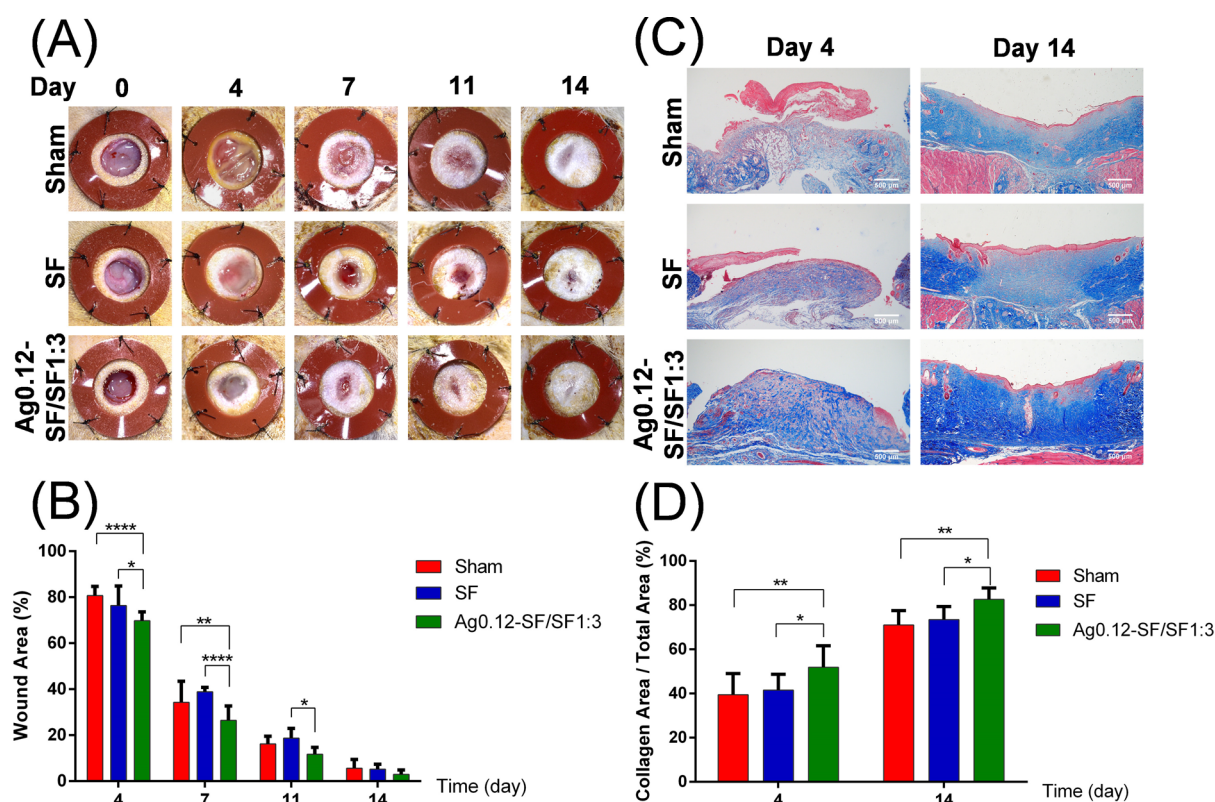


Figure 7. Representative macroscopic images and Masson staining images of wounds. (A) Representative photos of wounds of sham, SF, and Ag0.12-SF/SF1:3 groups on days 0, 4, 7, 11, and 14 after surgery. (B) Quantitative analysis of the percentage of the remaining wound area from macroscopic images. (C) Masson staining images of three groups on days 4 and 14 after surgery. (D) Quantitative analysis of collagen formation in the wound area in three groups. * $P < 0.05$, ** $P < 0.01$, and **** $P < 0.0001$.

such cellular organelles.^{12,13} Therefore, the Ag0.12-SF/SF1:3 membranes were adopted for further experiments.

2.6. Scratch Wound Healing Test on SF and Ag-SF/SF Membranes. The *in vitro* wound healing effect of SF and Ag-SF/SF membranes on HFFs was evaluated by the scratch wound healing test. As shown in Figure 6A–F, after scratching, the tissue culture plate (TCP), SF membrane, and the SF side of Ag0.12-SF/SF1:3 membrane groups all showed a scratched line without cells. Due to the flexibility of SF membranes, the lines from the SF membranes and the SF side of Ag0.12-SF/SF1:3 membranes were wider than those on TCP immediately after scratching. Regardless of these discrepancies, both the SF membranes and the SF side of Ag0.12-SF/SF1:3 membranes showed similar *in vitro* wound closure to the TCP group. Therefore, SF membranes and the SF side of Ag0.12-SF/SF1:3 membranes may promote wound healing.

2.7. Expression of Col I and TGF- β of HFFs on Ag-SF/SF Membranes. Col I is a major component of ECM and a natural substrate for cell attachment, growth, and differentiation.^{37,38} TGF- β can regulate cell proliferation, migration, differentiation, and the production of ECM and play a multi-effect role in wound healing.³⁹ Therefore, the expression levels of Col I and TGF- β were further assessed to explore the potential of the Ag-SF/SF membranes on skin regeneration. As shown in Figure 6G,H, after cultured for 7 days, the expression levels of Col I and TGF- β in cells cultured on SF membranes and the SF sides of Ag0.12-SF/SF1:3 membranes were higher than those on TCP. It indicated that the addition of Ag could still make membranes exert the function of promoting wound healing. The promotion of Col I and TGF- β expression

indicated that both SF membranes and Ag0.12-SF/SF1:3 membranes could facilitate wound healing.

2.8. *In Vivo* Wound Healing of Ag-SF/SF Membranes.

To evaluate whether the membranes could promote skin wound healing, a rat excisional wound splinting model challenged with *S. aureus* was adopted. All splints standardized the wound area during 14 days (Figure 7A). Although all wounds healed to more than 90% in 14 days, the healing rate of the Ag0.12-SF/SF1:3 group was significantly faster than that of sham and SF groups (Figure 7B). Masson staining showed that collagen formation in the Ag0.12-SF/SF1:3 group was more than that in both sham and SF groups (Figure 7C,D). In total, 50% of new collagen was found in the Ag0.12-SF/SF1:3 group on day 4, and the new collagen could reach 80% on day 14. The results showed that Ag0.12-SF/SF1:3 membranes significantly promoted the healing of infected wounds with more collagen formation. It could be mainly attributed to the synergistic effect of the antibacterial properties of Ag and the healing-promoting properties of SF.^{40,41} The bacterial infection could aggravate wound inflammation and increase matrix metalloproteinases, which mainly participated in the degradation of ECM.^{42,43} On this account, combating bacterial infection could reduce both the bacterial burden and inflammation and accumulate ECM, which could eventually accelerate wound healing. Besides, SF was reported to promote wound healing by activating the classic NF- κ B signaling pathway,⁴⁴ promoting the collagen synthesis of fibroblasts and upregulating TGF- β expression.^{45,46} Therefore, the unilateral Ag-SF/SF membranes might have great potential as antibacterial wound dressings. Ag-SF/SF membranes might have

the potential to treat chronic infectious wounds, especially wounds that cannot heal for a long time. Since chronic wounds are often accompanied by infection,⁴⁷ Ag-SF/SF membranes have both antibacterial and healing effects, which could effectively treat chronic infectious wounds.

3. CONCLUSIONS

Ag-SF/SF difunctional membranes were successfully fabricated through a simplified layer-by-layer technique. Both sides of the Ag-SF/SF membrane exerted an antibacterial effect, and the SF side promoted wound healing efficiently. The Ag-SF/SF membranes with doses of more than 0.06 mg/mL Ag could exert effective and comparable antibacterial properties on both sides. Meanwhile, studies on cell viability revealed that Ag0.12-SF/SF1:3 membranes had good cytocompatibility on the SF side while holding strong antibacterial properties. Besides, the Ag0.12-SF/SF1:3 membranes could promote the expression levels of Col I and TGF- β mRNA *in vitro* and significantly enhance the healing of infected wounds *in vivo*. Therefore, our research provided a new strategy to enlarge the therapeutic window for Ag-containing wound dressings by the simplified layer-by-layer technique to achieve Ag unilateral distribution. The prepared Ag-SF/SF difunctional membranes have great potential as wound dressings for efficient skin repair.

4. MATERIALS AND METHODS

4.1. Materials and Agents. All chemical reagents were of analytical grade and used without any further purification. Formic acid (88%), calcium chloride (96.0%, CaCl₂), sodium carbonate (99.8%, Na₂CO₃), AgNO₃ (99.8%), and anhydrous ethanol (99.7%) were purchased from Sinopharm (Shanghai, China). Silkworm cocoons were purchased from the northwest silkworm base (Ankang, Shanxi, China).

4.2. Preparation and Fabrication of Ag-SF/SF Membranes. The degumming process of silk was in accordance with a previous study.⁴⁸ The degummed SF was dissolved in the CaCl₂/formic acid solution to form the SF solution. AgNO₃ was dissolved in the SF solution to form the Ag-SF solution. The concentration of the Ag element was calculated based on the amounts of AgNO₃ dissolved in the solutions. Ag-SF solutions (200 μ L) with the 0.03–0.24 mg/mL concentration of the Ag element were dispersed over the entire mold (ϕ 35 mm), which were volatilized in the fume hood for 0.5 h, and then 600 μ L of SF solutions was added and dried for another 2.5 h. For the membranes with different thickness ratios, 200 μ L of Ag-SF solutions with 0.12 mg/mL concentration of the Ag element was thence-molded with 600, 1000, or 1400 μ L of SF solution according to the same procedure. The molds with membranes were dipped in distilled water for 0.5 h and then immersed in absolute ethanol for 1–2 h to release the mold. The thicknesses of membranes were 0.3–0.6 mm, and the membranes were cut into ϕ 10-mm samples with a punch for further usage. The membranes were named based on the combination of the Ag element concentration in the Ag-SF solutions and the Ag-SF/SF layer ratios, e.g., Ag0.12-SF/SF1:3 means that the two-layered membranes with an Ag-SF/SF layer ratio of 1:3 and the Ag element concentration in the Ag-SF solution of 0.12 mg/mL.

4.3. Characterization of Membranes. The Ag-SF/SF membranes used for characterization tests were Ag0.12-SF/SF1:3. The morphology of SF and Ag-SF/SF membranes was

observed under a SEM (Phenom ProX, G5, Eindhoven, Netherlands). The element distribution of Ag-SF/SF membranes was analyzed via EDX mapping on SEM. XRD patterns were recorded on a Bruker D8 advanced powder diffractometer (Bruker, Karlsruhe, Baden-Württemberg, Germany). FTIR spectra were obtained under a Thermo Nexus 670 spectrometer (Thermo Nicolet, Laporte, Colorado). The tensile properties of membranes ($n = 3$) were tested by a universal testing machine (Instron 3340, Boston, MA).

4.4. Ag⁺ Release from Ag-SF/SF Membranes. Ag-SF/SF (Ag0.12-SF/SF1:3) membranes ($n = 3$) were incubated in 2 mL of phosphate-buffered solution (PBS, Hyclone, Logan, Utah) (pH 7.2–7.4) with 100 rpm constant agitation at 37 °C. At 1, 6, 24, 72, 168, 240, and 336 h, 2 mL of supernatant was collected separately and replaced with fresh PBS. The concentration of Ag⁺ was estimated by atomic absorption spectroscopy (AAS) analysis (iCE 3500, Thermo Fisher Scientific, Waltham, MA) to assess the release profile.

4.5. In Vitro Antibacterial Test. A ZOI test was adopted to evaluate the antibacterial efficiency against typical pathogenic bacteria in skin wounds, i.e., *S. aureus* (ATCC 6538, Guangdong Microbial Culture Center, Guangzhou, Guangdong, China) and *E. coli* (ATCC 25922, Manassas, VA).³⁴ The bacterial suspension was made in the following steps: the single colonies of *S. aureus* or *E. coli* strain were swabbed on the agar plates, added to 10 mL of sterile saline (0.85% w/v NaCl in water), and then vortexed for 30 s. The bacterial suspension was further diluted to an OD_{600 nm} value of 0.123 to obtain the bacterial suspension concentration of 10⁸ CFU. Then, the bacterial suspension concentration was diluted to 10⁷ CFU. Afterward, the bacterial suspension was smeared evenly on the nutrient agar plate (composed of peptone, beef extract, NaCl, and agar powder) (BKM Biotechnology, Changde, Hunan, China) and the 10-mm-diameter disk samples ($n = 3$) were placed on the agar plates. Both the Ag-SF side and SF side of the membranes from different groups were placed on the agar plates, based on the purpose of the experiment. For example, in the Ag-SF side groups, the Ag-SF side of the samples contacted the agar plates, and in the SF side groups, the SF side of the samples contacted the agar plates. After cultivation for 20 h at 36 °C, the images were captured using a ruler as a calibrator and the diameters of the transparent inhibition zones were measured by ImageJ software (Open Source Software, OSS).

4.6. Cell Viability and Proliferation on SF and Ag-SF/SF Membranes. The HFFs were harvested from the human foreskin tissues provided by the Department of Urology, Qilu Hospital of Shandong University following the national guidelines for working with human materials. HFFs were acquired by enzymatic digestion and cultured in high-glucose Dulbecco's modified Eagle's medium (DMEM, Hyclone) with 10% fetal bovine serum (FBS, BioInd, Kibbutz, Israel) at 37 °C in a 5% CO₂ incubator. The membranes were preimmersed in the culture medium overnight. HFFs at a density of 3 \times 10⁴ cells/well were seeded onto SF or Ag-SF/SF membranes in 48-well plates. The cells were cultured in six replicates for each group. HFFs cultured on TCP served as the control. After 24 h, three replicate cells were observed qualitatively by the live/dead cells staining kit (Solarbio), the other three were digested and detached from the membranes and transferred to 96-well plates. After another 12 h, the culture medium in each well was refreshed with 10 μ L of CCK-8 (Dojindo Laboratories, Kumamoto, Japan) and 100 μ L of DMEM. The absorbance

Table 1. Primer Sequences for qRT-PCR

gene	forward primer (5'–3')	reverse primer (5'–3')
GAPDH	GCACCGTCAAGGCTGAGAAC	TGGTGAAGACGCCAGTGGA
Col I	GCCAAGACGAAGACATCCCA	GGCAGTTCTTGGTCTCGTCA
TGF- β	TTGACTTCCGCAAGGACCTC	CTCCAATGTAGGGGCAGGG

was detected by a microplate reader (SPEC-TROstar Nano, BMG Labtech, Offenburg, Germany) at a wavelength of 450 nm.

4.7. Scratch Wound Healing Test. HFFs at a density of 3×10^5 cells/well were seeded onto SF or Ag0.12-SF/SF1:3 membranes in six-well plates and cultivated in high-glucose DMEM with 10% FBS. HFFs cultured on TCP served as the control. After confluence, the monolayer HFFs were scratched by a sterile pipette tip and rinsed with PBS to remove cell debris. Then, cells were further cultured at 37 °C for 24 h. The wound healing photographs were taken at 0 and 24 h after the scratch.

4.8. RNA Isolation and qRT-PCR Analysis. HFFs at a density of 1×10^5 cells/well were seeded onto membranes ($n = 3$) in six-well plates and cultivated in high-glucose DMEM with 10% FBS for 7 days to detect gene expression of Col I and TGF- β . The medium was refreshed every 3 days. Total RNA was extracted by TRIzol reagent (Takara, Kusatsu, Japan). The mRNA was reversed-transcribed into cDNA. The quantitative real-time PCR assays were performed using SYBR Premix EX Taq II (Takara) with a Light Cycler Roche 480 II Real-Time PCR System (Roche, Basel, Switzerland). The housekeeping gene glyceraldehyde-3-phosphate dehydrogenase (GAPDH) was used to normalize the mRNA level of Col I and TGF- β . The sequences of the primers used in the present study are listed in Table 1.

4.9. Skin Excisional Wound Splinting Model Preparation. Animal experiments were approved by the Medical Ethics Committee of the School of Stomatology, Shandong University, Jinan, China (Protocol No: GR20200708). Twelve 8-week-old adult Wistar rats (200–250 g, male) were involved in this study. The blindness was conducted by keeping all sample group's information by an independent researcher (L.Y.), which was not made public until all of the data were collected. All wounds were randomly assigned to the three groups, i.e., sham control, SF, and Ag0.12-SF/SF1:3 groups ($n = 8$). The sham control was the group with simply punched the skin and smeared the bacteria without placing the membrane. In the Ag0.12-SF/SF1:3 group, the SF side of the membranes contacted the wounds. After inhalation of anesthesia with isoflurane, the rat's back hair was shaved off and then the surgical area was cleaned with iodophor and 75% ethanol in turn. Four circular wounds of 8-mm-diameter were punched on both sides of the back skin with disposable biopsy punches (Kai Industries Co. Ltd., Gifu, Japan). A red round silicone pad (inside diameter 12 mm, outside diameter 22 mm, thickness 1 mm) was glued to the skin around the wound and secured by sutures to prevent wound closure from contraction of the skin. Afterward, 10 μ L of bacterial suspension of *S. aureus* (1×10^8 CFU) in 0.85% sterile saline was injected into the wound surfaces and covered by different samples (ϕ 10 mm disk). Then, the four wounds on the back skin of rats were wrapped with 3M Tegaderm dressings (St. Paul, MN) and finally fixed with twining bandages (3M Deutschland GmbH, Neuss, Germany). On 0, 4, 7, 11, and 14 days postsurgery, wound healing photographs were taken. The rats were euthanized with

an overdose of pentobarbital on days 4 and 14, and the wounds along with the surrounding normal skins were collected and kept in 4% paraformaldehyde. The wound reduction was quantified using a method according to our previous study.⁴⁹ The wound area (%) was expressed as the wound reduction using the following equation

$$\text{wound area (\%)} = \frac{\text{wound area at day } X}{\text{wound area at day } 0} \times 100\%$$

4.10. Histological Analysis. The samples were dehydrated through graded series of ethanol and embedded in paraffin. The continuous cross sections of 5 μ m thickness were cut along the superficial to the deep layer of the skin. Every 19th section was stained with Masson's trichrome (Solarbio). All samples were observed under a BX53 microscope (Olympus, Tokyo, Japan) and measured with ImageJ software (OSS). The collagen formation was quantified using the collagen volume fraction (CVF).⁵⁰ The area of blue-dyed tissue was considered as the collagen area. CVF was expressed as the collagen area/total area (%) and calculated as the area occupied by the blue-dyed tissue, divided by the total area under direct vision.

4.11. Statistical Analysis. All data were shown as mean \pm standard deviation (SD) and analyzed by GraphPad Prism software 6.0 (MacKiev Software, Boston, MA). One-way or two-way ANOVA followed by the Tukey posthoc test was used to analyze the statistical significance. $P < 0.05$ was considered statistically significant.

AUTHOR INFORMATION

Corresponding Authors

Baojin Ma – Department of Periodontology, School and Hospital of Stomatology, Shandong University & Shandong Key Laboratory of Oral Tissue Regeneration & Shandong Engineering Laboratory for Dental Materials and Oral Tissue Regeneration, Jinan, Shandong 250012, China; Email: baojinma@sdu.edu.cn

Shaohua Ge – Department of Periodontology, School and Hospital of Stomatology, Shandong University & Shandong Key Laboratory of Oral Tissue Regeneration & Shandong Engineering Laboratory for Dental Materials and Oral Tissue Regeneration, Jinan, Shandong 250012, China; orcid.org/0000-0003-3821-5480; Email: shaohuage@sdu.edu.cn

Authors

Jinlong Shao – Department of Periodontology, School and Hospital of Stomatology, Shandong University & Shandong Key Laboratory of Oral Tissue Regeneration & Shandong Engineering Laboratory for Dental Materials and Oral Tissue Regeneration, Jinan, Shandong 250012, China; orcid.org/0000-0001-8684-4666

Yating Cui – Department of Periodontology, School and Hospital of Stomatology, Shandong University & Shandong Key Laboratory of Oral Tissue Regeneration & Shandong Engineering Laboratory for Dental Materials and Oral Tissue Regeneration, Jinan, Shandong 250012, China

Ye Liang – Department of Periodontology, School and Hospital of Stomatology, Shandong University & Shandong Laboratory of Oral Tissue Regeneration & Shandong Engineering Laboratory for Dental Materials and Oral Tissue Regeneration, Jinan, Shandong 250012, China

Hong Liu – State Key Laboratory of Crystal Materials, Shandong University, Jinan, Shandong 250100, China;
orcid.org/0000-0003-1640-9620

Complete contact information is available at:

<https://pubs.acs.org/10.1021/acsomega.1c02035>

Author Contributions

§J.S. and Y.C. contributed equally to this work and should be regarded as co-first authors. J.S.: study design, data curation, formal analysis, methodology, software, validation, and writing—review and editing. Y.C.: data curation, formal analysis, methodology, writing—original draft. Y.L.: methodology and software. H.L.: software and formal analysis. B.M.: conceptualization, resources, and writing—review and editing. S.G.: conceptualization, funding acquisition, resources, supervision, and writing—review and editing.

Notes

The authors declare no competing financial interest.

ACKNOWLEDGMENTS

This research was supported by the National Natural Science Foundation of China (Nos. 81670993, 81873716, and 81901009), the Construction Engineering Special Fund of “Taishan Scholars” of Shandong Province (Nos. ts20190975 and tsqn201909180), China Postdoctoral Science Foundation (Nos. 2019M652409 and 2019TQ0187), Shandong Provincial Postdoctoral Innovation Project (202001009), the National Key R&D Program of China (No. 2017YFB0405400), Jinan Medicine and Health Science Technology Project (No. 201907090), the Collaborative Innovation Center of Technology and Equipment for Biological Diagnosis and Therapy in Universities of Shandong, and the National Key Research and Development Program of China (No. 2017YFA0104604). The funding agencies have no role in study design, data collection and analysis, decision to publish, or preparation of the manuscript.

REFERENCES

- (1) Qi, Y.; Wang, H.; Wei, K.; Yang, Y.; Zheng, R. Y.; Kim, I. S.; Zhang, K. Q. A review of structure construction of silk fibroin biomaterials from single structures to multi-level structures. *Int. J. Mol. Sci.* **2017**, *18*, No. 237.
- (2) Jao, D.; Mou, X.; Hu, X. Tissue regeneration: a silk road. *J. Funct. Biomater.* **2016**, *7*, No. 22.
- (3) Lu, G.; Ding, Z.; Wei, Y.; Lu, X.; Lu, Q.; Kaplan, D. L. Anisotropic biomimetic silk scaffolds for improved cell migration and healing of skin wounds. *ACS Appl. Mater. Interfaces* **2018**, *10*, 44314–44323.
- (4) Vasconcelos, A.; Cavaco-Paulo, A. Wound dressings for a proteolytic-rich environment. *Appl. Microbiol. Biotechnol.* **2011**, *90*, 445–460.
- (5) Chouhan, D.; Mandal, B. B. Silk biomaterials in wound healing and skin regeneration therapeutics: from bench to bedside. *Acta Biomater.* **2020**, *103*, 24–51.
- (6) Han, L.; Li, P. F.; Tang, P. F.; Wang, X.; Zhou, T.; Wang, K. F.; Ren, F. Z.; Guo, T. L.; Lu, X. Mussel-inspired cryogels for promoting wound regeneration through photobiostimulation, modulating inflammatory responses and suppressing bacterial invasion. *Nanoscale* **2019**, *11*, 15846–15861.

(7) Song, D. W.; Kim, S. H.; Kim, H. H.; Lee, K. H.; Ki, C. S.; Park, Y. H. Multi-biofunction of antimicrobial peptide-immobilized silk fibroin nanofiber membrane: implications for wound healing. *Acta Biomater.* **2016**, *39*, 146–155.

(8) Vieira, D.; Angel, S.; Honjol, Y.; Gruenheid, S.; Gbureck, U.; Harvey, E.; Merle, G. Electroceutical silk-silver gel to eradicate bacterial infection. *Adv. Biosyst.* **2020**, *4*, No. 1900242.

(9) Hadisi, Z.; Farokhi, M.; Bakhsheshi-Rad, H. R.; Jahanshahi, M.; Hasanpour, S.; Pagan, E.; Dolatshahi-Pirouz, A.; Zhang, Y. S.; Kundu, S. C.; Akbari, M. Hyaluronic acid (HA)-based silk fibroin/zinc oxide core-shell electrospun dressing for burn wound management. *Macromol. Biosci.* **2020**, *20*, No. 1900328.

(10) Cutting, K.; White, R.; Edmonds, M. The safety and efficacy of dressings with silver - addressing clinical concerns. *Int. Wound J.* **2007**, *4*, 177–184.

(11) Greulich, C.; Braun, D.; Peetsch, A.; Diendorf, J.; Siebers, B.; Epple, M.; Koller, M. The toxic effect of silver ions and silver nanoparticles towards bacteria and human cells occurs in the same concentration range. *RSC Adv.* **2012**, *2*, 6981–6987.

(12) Lu, T.; Qu, Q.; Lavoie, M.; Pan, X. J.; Peijnenburg, W. J. G. M.; Zhou, Z. G.; Pan, X. L.; Cai, Z. Q.; Qian, H. F. Insights into the transcriptional responses of a microbial community to silver nanoparticles in a freshwater microcosm. *Environ. Pollut.* **2020**, *258*, No. 113727.

(13) Hrkac, T.; Rohl, C.; Podschun, R.; Zaporozhtchenko, V.; Strunskus, T.; Papavlassopoulos, H.; Garbe-Schonberg, D.; Faupel, F. Huge increase of therapeutic window at a bioactive silver/titania nanocomposite coating surface compared to solution. *Mater. Sci. Eng., C* **2013**, *33*, 2367–2375.

(14) Abram, S. L.; Fromm, K. M. Handling (nano)silver as antimicrobial agent: therapeutic window, dissolution dynamics, detection methods and molecular interactions. *Chem. - Eur. J.* **2020**, *26*, 10948–10971.

(15) Liao, C. Z.; Li, Y. C.; Tjong, S. C. Bactericidal and cytotoxic properties of silver nanoparticles. *Int. J. Mol. Sci.* **2019**, *20*, No. 449.

(16) Rashaan, Z. M.; Krijnen, P.; Klamer, R. R. M.; Schipper, I. B.; Dekkers, O. M.; Breederveld, R. S. Nonsilver treatment vs. silver sulfadiazine in treatment of partial-thickness burn wounds in children: a systematic review and meta-analysis. *Wound Repair Regen.* **2014**, *22*, 473–482.

(17) Atiyeh, B. S.; Costagliola, M.; Hayek, S. N.; Dibo, S. A. Effect of silver on burn wound infection control and healing: review of the literature. *Burns* **2007**, *33*, 139–148.

(18) Lin, Y. H.; Hsu, W. S.; Chung, W. Y.; Ko, T. H.; Lin, J. H. Evaluation of various silver-containing dressing on infected excision wound healing study. *J. Mater. Sci.: Mater. Med.* **2014**, *25*, 1375–1386.

(19) Thomason, H. A.; Lovett, J. M.; Spina, C. J.; Stephenson, C.; McBain, A. J.; Hardman, M. J. Silver oxysalts promote cutaneous wound healing independent of infection. *Wound Repair Regen.* **2018**, *26*, 144–152.

(20) Khorrami, S.; Zarrabi, A.; Khaleghi, M.; Danaei, M.; Mozafari, M. R. Selective cytotoxicity of green synthesized silver nanoparticles against the MCF-7 tumor cell line and their enhanced antioxidant and antimicrobial properties. *Int. J. Nanomed.* **2018**, *13*, 8013–8024.

(21) Ferreira, L. A. B.; Dos Reis, S. B.; do Nascimento da Silva, E.; Cadore, S.; Bernardes, J. D. S.; Duran, N.; de Jesus, M. B. Thiol-antioxidants interfere with assessing silver nanoparticle cytotoxicity. *Nanomedicine* **2020**, *24*, No. 102130.

(22) Zhang, H.; Yang, Z.; Ju, Y.; Chu, X.; Ding, Y.; Huang, X.; Zhu, K.; Tang, T.; Su, X.; Hou, Y. Galvanic displacement synthesis of monodisperse janus- and satellite-like plasmonic-magnetic Ag-Fe@Fe₃O₄ heterostructures with reduced cytotoxicity. *Adv. Sci.* **2018**, *5*, No. 1800271.

(23) Zhang, S.; Xing, M.; Li, B. Biomimetic layer-by-layer self-assembly of nanofilms, nanocoatings, and 3D scaffolds for tissue engineering. *Int. J. Mol. Sci.* **2018**, *19*, No. 1641.

(24) Liu, T.; Wang, Y.; Zhong, W.; Li, B.; Mequanint, K.; Luo, G.; Xing, M. Biomedical applications of layer-by-layer self-assembly for

cell encapsulation: current status and future perspectives. *Adv. Healthcare Mater.* **2019**, *8*, No. 1800939.

(25) Xie, Q. F.; Xu, Z. P.; Hu, B. H.; He, X. L.; Zhu, L. J. Preparation of a novel silk microfiber covered by AgCl nanoparticles with antimicrobial activity. *Microsc. Res. Tech.* **2017**, *80*, 272–279.

(26) Li, X. F.; Fan, Q. M.; Zhang, Q.; Yan, S. Q.; You, R. C. Freezing-induced silk I crystallization of silk fibroin. *CrystEngComm* **2020**, *22*, 3884–3890.

(27) Shang, L. L.; Ma, B. J.; Wang, F. L.; Li, J. H.; Shen, S.; Li, X. Y.; Liu, H.; Ge, S. H. Nanotextured silk fibroin/hydroxyapatite biomimetic bilayer tough structure regulated osteogenic/chondrogenic differentiation of mesenchymal stem cells for osteochondral repair. *Cell Proliferation* **2020**, *53*, No. e12917.

(28) Han, C. C.; Ge, L.; Chen, C. F.; Li, Y. J.; Zhao, Z.; Xiao, X. L.; Li, Z. L.; Zhang, J. L. Site-selected synthesis of novel Ag@AgCl nanoframes with efficient visible light induced photocatalytic activity. *J. Mater. Chem. A* **2014**, *2*, 12594–12600.

(29) Kim, M. H.; Park, W. H. Chemically cross-linked silk fibroin hydrogel with enhanced elastic properties, biodegradability, and biocompatibility. *Int. J. Nanomed.* **2016**, *11*, 2967–2978.

(30) Zhang, Y. W.; Jiang, M. M.; Zhang, Y. Q.; Cao, Q. P.; Wang, X.; Han, Y.; Sun, G. W.; Li, Y.; Zhou, J. H. Novel lignin-chitosan-PVA composite hydrogel for wound dressing. *Mater. Sci. Eng., C* **2019**, *104*, No. 110002.

(31) Leyva-Mendivil, M. F.; Page, A.; Bressloff, N. W.; Limbert, G. A mechanistic insight into the mechanical role of the stratum corneum during stretching and compression of the skin. *J. Mech. Behav. Biomed. Mater.* **2015**, *49*, 197–219.

(32) Sherman, V. R.; Tang, Y.; Zhao, S.; Yang, W.; Meyers, M. A. Structural characterization and viscoelastic constitutive modeling of skin. *Acta Biomater.* **2017**, *53*, 460–469.

(33) Su, D.; Yao, M.; Liu, J.; Zhong, Y.; Chen, X.; Shao, Z. Enhancing mechanical properties of silk fibroin hydrogel through restricting the growth of β -sheet domains. *ACS Appl. Mater. Interfaces* **2017**, *9*, 17489–17498.

(34) Shao, J. L.; Yu, N.; Kolwijck, E.; Wang, B.; Tan, K. W.; Jansen, J. A.; Walboomers, X. F.; Yang, F. Biological evaluation of silver nanoparticles incorporated into chitosan-based membranes. *Nano-medicine* **2017**, *12*, 2771–2785.

(35) Ponomarev, V. A.; Shvindina, N. V.; Permyakova, E. S.; Slukin, P. V.; Ignatov, S. G.; Sirota, B.; Voevodin, A. A.; Shtansky, D. V. Structure and antibacterial properties of Ag-doped micropattern surfaces produced by photolithography method. *Colloids Surf., B* **2019**, *173*, 719–724.

(36) Li, G.; Zhang, D. H.; Qin, S. H. Preparation and performance of antibacterial polyvinyl alcohol/polyethylene glycol/chitosan hydrogels containing silver chloride nanoparticles via one-step method. *Nanomaterials* **2019**, *9*, No. 972.

(37) Ruszczak, Z. Effect of collagen matrices on dermal wound healing. *Adv. Drug Delivery Rev.* **2003**, *55*, 1595–1611.

(38) Campos, A. C. L.; Groth, A. K.; Branco, A. B. Assessment and nutritional aspects of wound healing. *Curr. Opin. Clin. Nutr. Metab. Care* **2008**, *11*, 281–288.

(39) Lichtman, M. K.; Otero-Vinas, M.; Falanga, V. Transforming growth factor beta (TGF- β) isoforms in wound healing and fibrosis. *Wound Repair Regener.* **2016**, *24*, 215–222.

(40) Min, S.; Gao, X.; Han, C.; Chen, Y.; Yang, M.; Zhu, L.; Zhang, H.; Liu, L.; Yao, J. Preparation of a silk fibroin spongy wound dressing and its therapeutic efficiency in skin defects. *J. Biomater. Sci., Polym. Ed.* **2012**, *23*, 97–110.

(41) Yu, K.; Lu, F.; Li, Q.; Chen, H.; Lu, B.; Liu, J.; Li, Z.; Dai, F.; Wu, D.; Lan, G. In situ assembly of Ag nanoparticles (AgNPs) on porous silkworm cocoon-based wound film: enhanced antimicrobial and wound healing activity. *Sci. Rep.* **2017**, *7*, No. 2107.

(42) Edwards, R.; Harding, K. G. Bacteria and wound healing. *Curr. Opin. Infect. Dis.* **2004**, *17*, 91–96.

(43) Ramanathan, G.; Thyagarajan, S.; Sivagnanam, U. T. Accelerated wound healing and its promoting effects of biomimetic

collagen matrices with siderophore loaded gelatin microspheres in tissue engineering. *Mater. Sci. Eng., C* **2018**, *93*, 455–464.

(44) Park, Y. R.; Sultan, M. T.; Park, H. J.; Lee, J. M.; Ju, H. W.; Lee, O. J.; Lee, D. J.; Kaplan, D. L.; Park, C. H. NF- κ B signaling is key in the wound healing processes of silk fibroin. *Acta Biomater.* **2018**, *67*, 183–195.

(45) Roh, D. H.; Kang, S. Y.; Kim, J. Y.; Kwon, Y. B.; Young Kweon, H.; Lee, K. G.; Park, Y. H.; Baek, R. M.; Heo, C. Y.; Choe, J.; Lee, J. H. Wound healing effect of silk fibroin/alginate-blended sponge in full thickness skin defect of rat. *J. Mater. Sci.: Mater. Med.* **2006**, *17*, 547–552.

(46) Ju, H. W.; Lee, O. J.; Lee, J. M.; Moon, B. M.; Park, H. J.; Park, Y. R.; Lee, M. C.; Kim, S. H.; Chao, J. R.; Ki, C. S.; Park, C. H. Wound healing effect of electrospun silk fibroin nanomatrix in burn-model. *Int. J. Biol. Macromol.* **2016**, *85*, 29–39.

(47) Powers, J. G.; Higham, C.; Broussard, K.; Phillips, T. J. Wound healing and treating wounds: chronic wound care and management. *J. Am. Acad. Dermatol.* **2016**, *74*, 607–625. quiz 625–606.

(48) Chen, Y.; Wu, T.; Huang, S.; Suen, C. W.; Cheng, X.; Li, J.; Hou, H.; She, G.; Zhang, H.; Wang, H.; Zheng, X.; Zha, Z. Sustained release SDF-1 α /TGF- β 1-loaded silk fibroin-porous gelatin scaffold promotes cartilage repair. *ACS Appl. Mater. Interfaces* **2019**, *11*, 14608–14618.

(49) Shao, J. L.; Wang, B.; Li, J. M.; Jansen, J. A.; Walboomers, X. F.; Yang, F. Antibacterial effect and wound healing ability of silver nanoparticles incorporation into chitosan-based nanofibrous membranes. *Mater. Sci. Eng., C* **2019**, *98*, 1053–1063.

(50) Lai, S. Q.; Fu, X. Y.; Yang, S. F.; Zhang, S. T.; Lin, Q. X.; Zhang, M. Z.; Chen, H. M. G protein-coupled receptor kinase-2: a potential biomarker for early diabetic cardiomyopathy. *J. Diabetes* **2020**, *12*, 247–258.